Critical Power in Three-Core Photonic Crystal Fibers

Alanio Ferreira de Lima, Francisco Leonardo Bezerra Martins, José Cláudio do Nascimento, and Amarílio Gonçalves Coêlho, Jr.

***Abstract*— When a photonic crystal fiber has more than one core, the switching capacity loss among the cores as of a given power, called critical power, becomes a relevant effect for switching applications. In this paper, we study the critical power obtained when ultrashort pulses are propagated in a nonlinear directional coupler. Here, we consider the specific example of a three-core photonic crystal fiber in two possible arrangements: one-dimensional and triangular array. In each core, the pulses propagate in the anomalous dispersion regime, in which an input pulse in the form of a hyperbolic secant is injected into one of the cores, considering different input peak powers. By relating the group velocity dispersion and the coupling coefficient with the temporal width of the input pulse, we can observe some relations between the fiber parameters and the critical power. In addition, we show that when self-phase modulation is combined with other effects, the critical power can be increased or decreased depending on the combination of these effects.**

***Index Terms*— Photonic crystal fiber, critical power, nonlinear directional coupler.**

I. Introduction

A PHOTONIC Crystal Fiber (PCF) derives its properties from the geometric composition of an arrangement of small, slightly spaced, air-holes that pass through its entire length. These fibers offer many degrees of freedom in its design to achieve a variety of peculiar properties such as photonic bandgap, [1], [2], dispersion control [3], endless single-mode operation [4] and super-continuum generation [5].

Some interesting effects only appear in the PCF when it has more than one core [6]–[10]. One of these effects is the switching capacity loss that appears as of a given power, called the critical power, P_C. When propagating high power pulses, self-phase modulation induces distinct phases between the cores so that the high phase difference between the cores confines the light in the same core in which it was initially launched. This effect causes a symmetrical coupler to behave as an asymmetric coupler [11]. This phenomenon was experimentally investigated in two-core fibers [12], [13]. When considering the input beam as a constant signal, an analytical solution for the critical power can be found [11]. When analyzing ultrashort pulses in the presence of positive group velocity dispersion (GVD), power-dependent switching between two modes occurs only when the width of the input pulse is greater than a fundamental lower limit [14].

In this paper we study the behavior of the critical power in three-core PCFs under anomalous dispersion regime, ($\beta_2 < 0$). We related the group velocity dispersion, β_2, and the coupling coefficient, κ, to the temporal width parameter, i.e, $T_0 = 0.7625\sqrt{|\beta_2|/\kappa}$. In these conditions we note that

$$\frac{\sqrt{\kappa|\beta_2|}}{\gamma} \text{ is directly related to } P_C.$$

This relation agrees with several known facts: (1) an increase in the coupling constant (caused, for example, by the proximity between the cores) and/or (2) in the group velocity dispersion, causes an increase in the critical power of a PCF; on the other hand, (3) the decrease of the effective area (and consequent increase of the γ parameter, which refers to self-phase modulation) decreases the critical power in a PCF. In addition, when we combine self-phase modulation with other effects (Raman scattering, self-steepening and coupling coefficient dispersion), we note that the critical power increases or decreases depending on the combination of these effects.

The results obtained here are important for finding the critical power in switching-dependent three-core PCF applications such as logic gates [15]–[17] and power bandwidth controllers [18]. This is also useful for future investigations of models that describe in more detail the critical power.

This paper is divided as follows. In Section II, we present a theoretical model necessary for the understanding of the formation of the critical power. In Section III, we present the method for calculating the critical power. In Section IV, we show how we obtain the relations of β_2, κ and γ to the critical power. In Section V, we show how other effects influence the value of the critical power along with the self-phase modulation. In Section VI, we show how the temporal width, independent of fiber parameters, also influences the critical power. Finally, in Section VII, we present some conclusions.

II. Theoretical Model

The photonic crystal fiber (PCF) is formed by materials with low and high refractive indexes. Generally, the material which

Manuscript received October 30, 2017; revised January 10, 2018; accepted January 25, 2018. Date of publication February 9, 2018; date of current version March 8, 2018. This work was supported by Brazilian Agency FUNCAP. *(Corresponding author: José Cláudio do Nascimento.)*

A. F. de Lima, F. L. B. Martins, and J. C. do Nascimento are with the Department of Electrical and Computer Engineering, Universidade Federal do Ceará, Sobral 62010-560, Brazil (e-mail: allanio007@gmail.com; leonardobluesummers@gmail.com; claudio@sobral.ufc.br).

A. G. Coêlho Jr. is with the Telecommunications and Materials Science and Engineering Laboratory, Physics Department and Teleinformatics Engineering Department, Universidade Federal do Ceará–UFC, Fortaleza 60455-760, Brazil (e-mail: amariliofisica@yahoo.com.br).

Color versions of one or more of the figures in this paper are available online at http://ieeexplore.ieee.org.

Digital Object Identifier 10.1109/JQE.2018.2804344

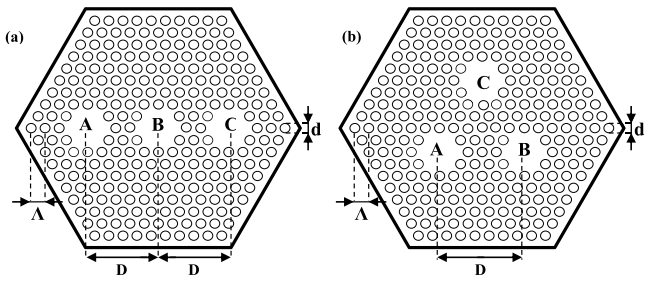

Fig. 1. Schematic of the three-core photonic crystal fiber - (a) one-dimensional array and (b) triangular array.

composes the core of the PCF is non-doped silica. The low refractive index region is composed of a periodic array of air holes with diameter d, distance between adjacent cores D, and hole-to-hole spacing $\Lambda = d/0.9$ (see Figure 1).

In Figure 1 we present two possible designs for the three-core PCF: (a) one-dimensional array and (b) triangular array. Both can be represented by a nonlinear directional coupler (NLDC). This offers us possibilities for switching, routing and modulation of optical signals when under nonlinear interaction in the coupling region between the wave guides [19], [20]. For each core we consider the dispersive effects of second and third order and several nonlinear effects such as self-phase modulation (SPM), cross-phase modulation (XPM), self-steepening (SS), Raman scattering and coupling dispersion. Like this, the propagation in the one-dimensional array coupler is described by the coupled mode equations 1-3, as shown below:

$$\begin{aligned} & i\frac{\partial a_1}{\partial z} - \frac{\beta_2}{2}\frac{\partial^2 a_1}{\partial t^2} - i\frac{\beta_3}{6}\frac{\partial^3 a_1}{\partial t^3} \\ & \quad + \gamma\left(|a_1|^2 + \eta|a_2|^2\right)a_1 + i\frac{\gamma}{\omega}\frac{\partial(|a_1^2|a_1)}{\partial t} \\ & \quad - \gamma a_1 T_R\frac{\partial(|a_1|^2)}{\partial t} + \kappa a_2 + i\kappa_1\frac{\partial(a_2)}{\partial t} = 0 \end{aligned} \tag{1}$$

$$\begin{aligned} & i\frac{\partial a_2}{\partial z} - \frac{\beta_2}{2}\frac{\partial^2 a_2}{\partial t^2} - i\frac{\beta_3}{6}\frac{\partial^3 a_2}{\partial t^3} \\ & \quad + \gamma\left(|a_2|^2 + \eta|a_1 + a_3|^2\right)a_2 + i\frac{\gamma}{\omega}\frac{\partial(|a_2^2|a_2)}{\partial t} \\ & \quad - \gamma a_2 T_R\frac{\partial(|a_2|^2)}{\partial t} + \kappa(a_1 + a_3) \\ & \quad + i\kappa_1\frac{\partial(a_1 + a_3)}{\partial t} = 0 \end{aligned} \tag{2}$$

$$\begin{aligned} & i\frac{\partial a_3}{\partial z} - \frac{\beta_2}{2}\frac{\partial^2 a_3}{\partial t^2} - i\frac{\beta_3}{6}\frac{\partial^3 a_3}{\partial t^3} \\ & \quad + \gamma\left(|a_3|^2 + \eta|a_2|^2\right)a_3 + i\frac{\gamma}{\omega}\frac{\partial(|a_3^2|a_3)}{\partial t} \\ & \quad - \gamma a_3 T_R\frac{\partial(|a_3|^2)}{\partial t} + \kappa a_2 \\ & \quad + i\kappa_1\frac{\partial(a_2)}{\partial t} = 0 \end{aligned} \tag{3}$$

Here, the PCF cores are considered to be identical. Furthermore, in Figure 1(b), the cores are considered to be equidistant among themselves. The propagation in the triangular coupler is described by the coupled equations 4-6, as shown below:

$$\begin{aligned} & i\frac{\partial a_1}{\partial z} - \frac{\beta_2}{2}\frac{\partial^2 a_1}{\partial t^2} - i\frac{\beta_3}{6}\frac{\partial^3 a_1}{\partial t^3} \\ & \quad + \gamma\left(|a_1|^2 + \eta(|a_2|^2 + |a_3|^2)\right)a_1 + i\frac{\gamma}{\omega}\frac{\partial(|a_1^2|a_1)}{\partial t} \\ & \quad - \gamma a_1 T_R\frac{\partial(|a_1|^2)}{\partial t} + \kappa(a_2 + a_3) \\ & \quad + i\kappa_1\frac{\partial(a_2 + a_3)}{\partial t} = 0 \end{aligned} \tag{4}$$

$$\begin{aligned} & i\frac{\partial a_2}{\partial z} - \frac{\beta_2}{2}\frac{\partial^2 a_2}{\partial t^2} - i\frac{\beta_3}{6}\frac{\partial^3 a_2}{\partial t^3} \\ & \quad + \gamma\left(|a_2|^2 + \eta|a_1 + a_3|^2\right)a_2 + i\frac{\gamma}{\omega}\frac{\partial(|a_2^2|a_2)}{\partial t} \\ & \quad - \gamma a_2 T_R\frac{\partial(|a_2|^2)}{\partial t} + \kappa(a_1 + a_3) \\ & \quad + i\kappa_1\frac{\partial(a_1 + a_3)}{\partial t} = 0 \end{aligned} \tag{5}$$

$$\begin{aligned} & i\frac{\partial a_3}{\partial z} - \frac{\beta_2}{2}\frac{\partial^2 a_3}{\partial t^2} - i\frac{\beta_3}{6}\frac{\partial^3 a_3}{\partial t^3} \\ & \quad + \gamma\left(|a_3|^2 + \eta|a_1 + a_2|^2\right)a_3 + i\frac{\gamma}{\omega}\frac{\partial(|a_3^2|a_3)}{\partial t} \\ & \quad - \gamma a_3 T_R\frac{\partial(|a_3|^2)}{\partial t} + \kappa(a_1 + a_2) \\ & \quad + i\kappa_1\frac{\partial(a_1 + a_2)}{\partial t} = 0 \end{aligned} \tag{6}$$

Where t is the normalized retarded-time coordinate given by $t = t' - z/v_g$ (z is the distance along the fiber, t' is the current time and v_g is the group velocity); a_1, a_2 and a_3 are the amplitudes of the pulses launched into cores A, B and C, respectively; β_2 is the group velocity dispersion (GVD); β_3 is the third order dispersion (TOD); γ is the nonlinear parameter that accounts for the self-phase modulation (SPM); the term multiplied by γ/ω governs the effect known as self steepening (SS); T_R is the Raman scattering coefficient; κ is the coupling coefficient between identical and equally spaced cores; κ_1 is the coupling coefficient dispersion given by $\kappa_1 = \partial\kappa/\partial\omega$ (ω is the angular optical frequency); η is a small ratio that measures the relative importance of cross-phase modulation (XPM) with regard to SPM, so this parameter will be neglected in this work.

Since amorphous silica can be treated as a homogeneous material, the third order susceptibility leads to an intensity-dependent variation without material index [11]. Hence, in the fiber design process, nonlinearity can be increased by limiting the effective mode area. This limitation occurs through a smaller core diameter and higher index contrast.

In conventional fibers, the numerical aperture (NA) is unsatisfactory to confine the mode when using smaller diameter cores, this increases the effective area, resulting in comparatively small values of γ. On the other hand, due to its air-hole cladding, in silica PCFs, we can have much larger NAs when compared to conventional silica fibers [21].

By properly choosing the size and pattern (of the air hole matrix) of the PCF, the effective area can be reduced. Like this, the effective nonlinearity of the fiber can be increased by increasing the intensity of light within the fiber. This increases

the nonlinear phase variation during the propagation of the pulse. In a PCF, the field in materials with different nonlinear characteristics will overlap [22], and the modified definition of the effective mode nonlinear area is given by:

$$A_{eff} = \frac{n_2[\int\int E(x,y)\cdot E^*(x,y)dxdy]^2}{\int\int \bar{n}_2(x,y)[E(x,y)\cdot E^*(x,y)]^2 dxdy}. \quad (7)$$

Where $E(x,y)$ is the transverse electric field, $\bar{n}_2(x,y)$ is the nonlinear index coefficient of the material at position (x,y). Thus, the fiber effective nonlinearity, γ, is given by:

$$\gamma = \frac{2\pi n_2}{\lambda A_{eff}}. \quad (8)$$

Where A_{eff} is the effective mode area and λ is the wavelength of light.

III. Critical Power Calculation

When propagating low-power pulses in short propagation lengths, we can disregard the non-linear and dispersive effects in the couplers. Like this, equations 1-3 and 4-6 become linear and, assuming identical cores, the coupling constants are the same between any adjacent cores. Hence, we can analytically determine the transmissions of the pulses inserted into core A,

$$T_P = \frac{1}{4}(\cos(\sqrt{2}\kappa z)+1)^2 \quad \text{and} \quad T_T = \frac{1}{9}(4\cos(3\kappa z)+5)^2.$$

Where T_P and T_T are the transmissions to the one-dimensional and triangular array couplers, respectively. Here, we can note that the transmission is periodic in terms of the propagation length, so we are only interested in the first length, where the energy transmission is maximum, which occurs when $T_P = T_T = 0$. This length value is usually called coupling length, denoted by L_C. Under these conditions, we obtain $L_C = \pi/\sqrt{2}\kappa$ for the one-dimensional array coupler and $L_C = \pi/3\kappa$ for the triangular array coupler.

In possession of these L_C values, we can now fix these lengths in the fiber and vary the input pulse energy. At high energies, the transmission does not only depend on fiber length, but also on the pulse-intensity-dependent nonlinear effects. Thus, when studying the transmission in non-linear regime couplers, we must compare the input energy to the output energy of the pulse.

In hyperbolic secant shaped pulses $a(0,t) = \sqrt{P_0}\text{sech}(t/T_0)$, the energy is given by $E = 2P_0T_0$, so we must make amplitude and temporal width adjustments in order to control the input pulse energy. Defining the temporal width by $T_0 = 0.7625\sqrt{|\beta_2|/\kappa}$, the energy of the pulse is given by $E = 1.525\ P_0\sqrt{|\beta_2|/\kappa}$. Like this, we only have to find out the relation between the fiber parameters and the critical power, P_C. For this, we vary the input power, P_0, between 0 and $8\kappa/\gamma$, so we can study the transmission of energy from one core to the others after a propagation of length L_C and then find the critical power.

For the numerical study of the transmission, we solve the system of equations 1-3 and 4-6 through the Runge-Kutta fourth order method. After obtaining the solution, we calculate the energy of the pulses in the output cores to determine the transmission as defined below:

$$T_j = \frac{\int_{\infty}^{-\infty}|a_j(L_C,t)|^2 dt}{\int_{\infty}^{-\infty}|a_1(0,t)|^2 dt}. \quad (9)$$

Where $j = 1, 2$ and 3 is the numbering for each pulse in equations 1-3 and 4-6 in which each of these pulses are inserted into cores A, B and C, respectively. Here, signal $a_j(L_C,t)$ represents the output pulse j and T_j is its transmission curve along the coupling length L_C.

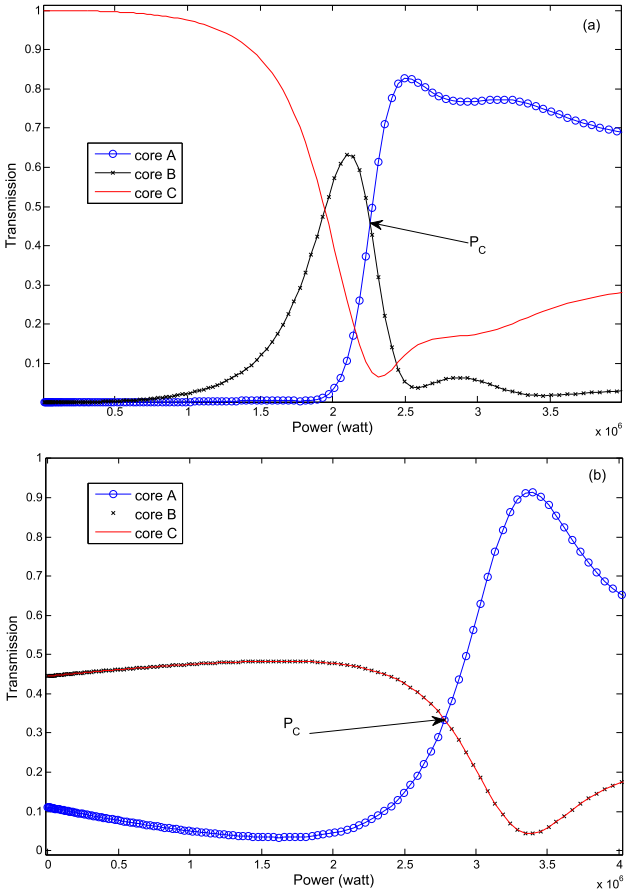

Fig. 2. Transmission vs peak power for a hyperbolic secant shaped pulse inserted into core A: (a) one-dimensional array coupler with $L_C = 2.53cm$ and (b) triangular array coupler with $L_C = 1.27cm$.

In Figure 2 we can observe the critical power points for the analyzed three-core couplers. Here, we set the fiber parameters as [7]: $\kappa = 87.266m^{-1}$, $\beta_2 = -47ps^2/km$, $\beta_3 = 0.1ps^3/km$, $\gamma = 3.2\times10^{-3}W^{-1}m^{-1}$. Under these conditions, self-phase modulation is the only nonlinear effect considered. In the one-dimensional array coupler, Figure 2 (a), the critical power point occurs at the intersection between the transmission curves of the cores A and B. After this point, the transmission curve exhibits small variations indicating a tendency of the energy to concentrate into core A, i.e., the light tends to remain into the core in which it was inserted. On the other hand, in the triangular array coupler, Figure 2 (b), the critical power point is located at the intersection of the three transmission curves. Here, after the point of intersection, the energy also exhibits a tendency to remain into the core in which the pulse has been inserted.

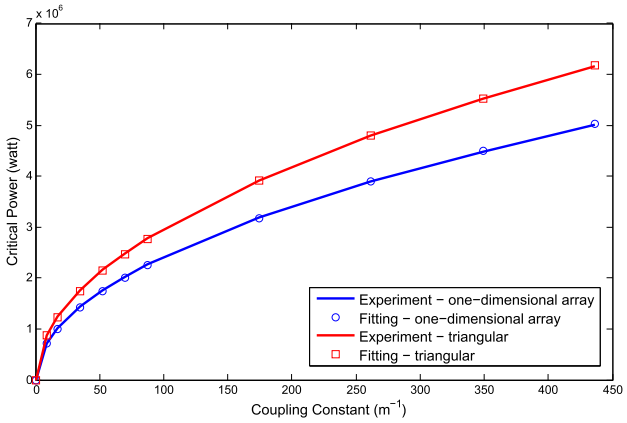

Fig. 3. P_C vs κ. The fitting is performed using equation 10. $a = 0.2408 Wm^{1/2}$ for the one-dimensional array coupler and $a = 0.2961 Wm^{1/2}$ for the triangular array coupler.

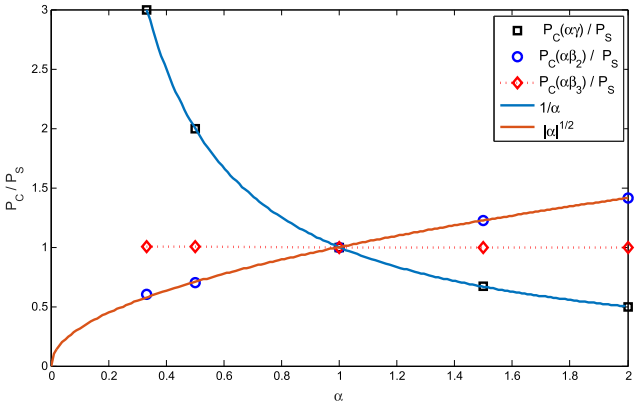

Fig. 4. Critical power normalized by P_S. α multiplies parameters γ, β_2, and β_3 one at a time in both couplers. The standard critical power is $P_S = 2.26MW$ for the one-dimensional array coupler and $P_S = 2.78MW$ for the triangular array coupler.

The knowledge of the critical power is essential to determine for which power values the coupler loses its switching capacity. When we launch an ultra short pulse into core A, SPM induces distinct phases between the cores so that the phase difference is high enough that the input beam remains confined to the same core in which it was initially launched. In Figure 2, considering ultra short pulses, the one-dimensional array coupler has $P_C = 2.26MW$, whereas the triangular array coupler has $P_C = 2.78MW$.

IV. Critical Power Considering Only SPM

Now, in order to understand how critical power depends on the fiber parameters, we vary the parameters of equations 1-3 and 4-6. Initially, we consider SPM, γ, as the only nonlinear effect along with the dispersive effects (β_2 and β_3) and the coupling constant, κ. The other nonlinear effects expressed in equations 1-3 and 4-6 will be discussed in the next section.

Taking the coupling constant, κ as the first parameter for study, we record the critical power values when κ is multiplied by the following factors: 0.1, 0.2, 0.4, 0.6, 0.8, 1, 2, 3, 4, and 5. When analyzing the P_C vs κ graph (see Figure 3), we note a concavity in the curves of the one-dimensional and triangular array couplers. We performed several tests using genetic algorithms and determined the best fitting curve as being the curve given by:

$$P_C(\kappa) = a\sqrt{\kappa}. \tag{10}$$

The obtained P_C vs κ curve, according to equation 10, is shown in Figure 3. As we can see, equation 10 gives us a good approximation to the values of the critical power as a function of κ. In this approach, the largest adjustment error observed was in the order of 4.11% for the one-dimensional array coupler and 4.73% for the triangular array coupler.

In Figure 4 we show the behavior of the critical power as a function of parameters γ, β_2, and β_3. Here we apply a methodology analogous to that used to determine the relation between the critical power and $\sqrt{\kappa}$. To determine the dependence of P_C on γ, we vary the value of γ using a multiplier parameter, α.

TABLE I
Numerical Error for Testing the Hypothesis Raised in Expression 11

α_1	α_2	α_3	error (triangular)	error (one-dimensional)
1	2	3/2	0.00093310	0.0012
1/5	3/2	2	0.00092704	0.0011
3/2	1	2	0.0030	0.0039
1	1/2	3/2	0.0037	0.0049
1/5	3/2	1/2	0.00032719	0.00038181

In this analysis we normalized this variation and observed the behavior of the $P_C(\alpha\gamma)/P_S$ curve. Here $P_S = P_C(\gamma, \beta_2, \beta_3)$ is the standard critical power, where the parameters γ, β_2 and β_3 are multiplied by 1. Each coupler has a different standard critical power value, consequently the values of $P_C(\alpha\gamma)/P_S$ depend only on the variation of α. Again, using genetic algorithms, we repeated the search procedure for the best fitting curve and we noted that $P_C(\alpha\gamma)/P_C(\gamma) \approx 1/\alpha$. Therefore, we numerically verified that P_C is related to $1/\gamma$. Finally, we repeated this same procedure for β_2 and β_3, and we noted that P_C is related to $\sqrt{|\beta_2|}$, but it is not affected by β_3, i.e., $P_C(\alpha\beta_3)/P_C(\beta_3) \approx 1$.

So far, each test was performed by varying only one parameter at a time. Finally, we varied the parameters simultaneously and found evidences that

$$P_C \text{ is related to } \frac{\sqrt{\kappa|\beta_2|}}{\gamma}. \tag{11}$$

To verify this hypothesis, we solve equations 1-3 and 4-6 using the following parameters: $\kappa' = \alpha_1\kappa$, $\gamma' = \alpha_2\gamma$, and $\beta_2' = \alpha_3\beta_2$. We assume some arbitrary rational values for α_1, α_2, and α_3. Like this, we calculated the error of this hypothesis by: $error = |P_C(\kappa', \gamma', \beta_2')/P_S - (\sqrt{\alpha_1|\alpha_3|})/\alpha_2|$. The low numerical errors, presented in Table I, is an evidence that the critical power is related to $\sqrt{\kappa|\beta_2|}/\gamma$.

V. Critical Power and Other Effects

The influence of the nonlinear effects among the fiber cores depends largely on the coupling coefficient, κ, which is dependent on the distance between the cores. The greater

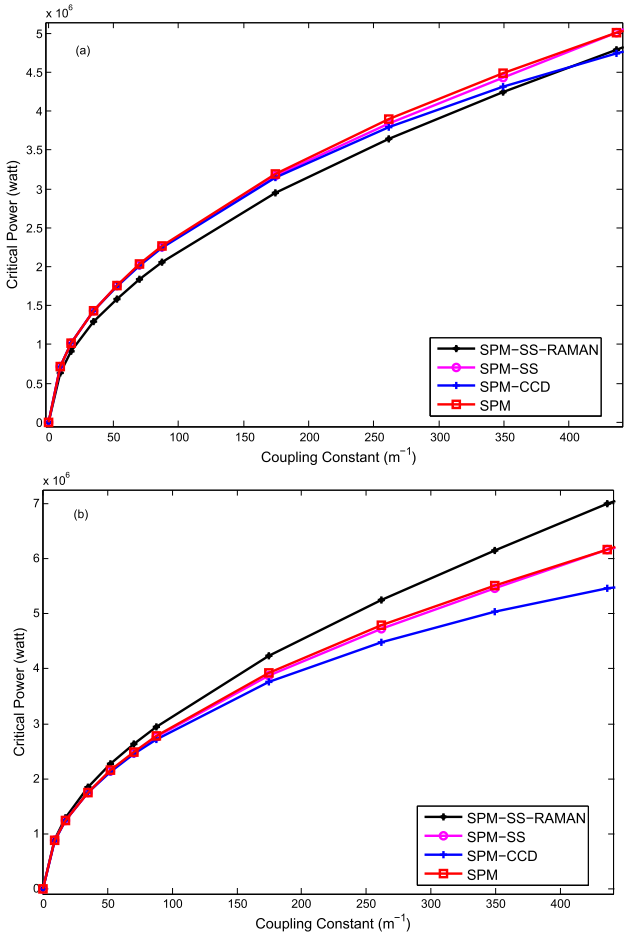

Fig. 5. P_C vs κ for the (a) one-dimensional and (b) triangular array coupler, when considering a hyperbolic secant shaped pulse inserted into core *A*. Each curve exhibits the behavior of P_C when considering combinations of the following nonlinear effects: coupling coefficient dispersion (CCD), self-phase modulation (SPM), self-stepenning (SS) and intrapulse stimulated Raman scattering (RAMAN).

the value of κ, the closer the cores are to each other and stronger is the influence of the light intensity between them. In Figure 5, we varied the coupling coefficient and added the nonlinear effects of self-steepening and intrapulse stimulated Raman scattering. We considered $\gamma = 3.2 \times W^{-1}m^{-1}$ and $T_R = T_0/10$, values adopted in [7] and [15]–[17]. Analyzing the curves in Figure 5, we note small deviations between the critical power vs coupling coefficient curves, which is an indication that combinations of nonlinear effects can decrease or increase the critical power.

In Figures 5 (a) and (b) we present the critical power vs coupling constant curves for the one-dimensional and triangular array couplers, respectively, when other effects (self-steepening, Raman scattering and coupling coefficient dispersion) are combined with SPM. Here, we note that the combination of the SPM and SS effects did not cause apparent changes in the critical power plot (due to the MW scale), however the difference between the curves is of order of $154kW$ for the one-dimensional array coupler and $67kW$ for the triangular array coupler. On the other hand, when we consider the effect of stimulated Raman scattering, we note a much more pronounced deviation. This can be observed

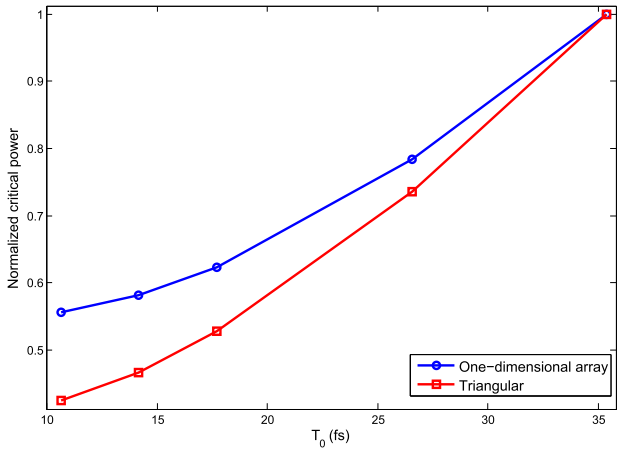

Fig. 6. Normalized critical power vs temporal width.

by comparing the SPM-SS-RAMAN curve to the SPM-SS and SPM curves in both couplers. For the one-dimensional array coupler, when considering the three effects (SPM-SS-RAMAN), we observed lower critical power values whereas for the triangular array coupler we observed higher critical power values.

Finally, the SPM-CCD curve in the Figures 5 (a) and (b) analyzes the influence of the coupling coefficient dispersion (CCD) on the critical power when this effect is combined with SPM. This analysis is relevant because when the pulse is ultrashort or the fiber is long enough, the coupling coefficient dispersion can cause pulse distortion or even pulse breakup [23]–[28]. These effects have been confirmed experimentally [29], [30]. Furthermore, it has been found that the coupling coefficient dispersion in a two-core PCF much shorter than one meter is sufficient to cause significant distortion for ultrashort input pulses [7]. In our simulations, we note (Figure 5 (a) and (b)) that the SPM-CCD curve tends to show greater concavity than the SPM curve when the power exceeds $3MW$. This is noted in the one-dimensional array to $\kappa > 160.75m^{-1}$ and in the triangular array to $\kappa > 110m^{-1}$.

As to the physical reasons for the behavior of SPM-CCD curve, firstly, we should emphasize that coupling coefficient dispersion effects are wave overlapping dependent, therefore the coupling geometry makes these effects stronger in triangular array than in one-dimensional array (see equations 1-6). Secondly, it should be noted that by varying the coupling constant κ, the coupling coefficient dispersion is also varied, since $\kappa_1 = \partial\kappa/\partial\omega$. Thus, the walk-off length, where we observe the first order coupling dispersion effects, decreases as much as κ grows [7], [23]. Therefore, when κ grows in Figures 5 (a) and (b), exceeding $160.75m^{-1}$ in the one-dimensional array and $110m^{-1}$ in the triangular array, the walk-off length gets close to the coupling length and the SPM-CCD concavity becomes stronger by revealing a lower growth of the critical power. Thus, we conclude that the CCD can decrease the switching capacity. This result is consistent with the transmission curves presented in [8], where the transmission curves are altered by coupling coefficient dispersion.

VI. Critical Power and Temporal Width

It has been demonstrated in [14] that there is a limit time width for which the coupler performs power-dependent switching. This is a clear evidence that the temporal width alters the critical power. In this section we show how, after this limit, the critical power varies for each time width. As a demonstration, we take four temporal widths T_0 between $10.61\,fs$ and $35.39\,fs$, independent of $\sqrt{|\beta_2|/\kappa}$. In Figure 6 we show the variations observed for the one-dimensional and triangular array couplers. Here, we note that when varying only T_0 (and no other parameters), the P_C curve is crescent with T_0, which proves that the temporal width changes the critical power.

VII. Conclusions

In multi-core photonic crystal fibers, when the power of the input pulse exceeds the critical power, the coupler loses its switching capacity, i.e., the pulse tends to remain into the core in which it was inserted. In this work we performed a study of how the critical power relates to the parameters of coupling constant, group velocity dispersion and self-phase modulation when ultrashort pulses are inserted into the fiber. Considering the anomalous dispersion regime ($\beta_2 < 0$), we initially related the GVD parameter, β_2, and the coupling coefficient, κ, to the temporal width parameter, i.e, $T_0 = 0.7625\sqrt{|\beta_2|/\kappa}$. Under these conditions we found numeric evidences that

$$\frac{\sqrt{\kappa|\beta_2|}}{\gamma} \text{ is directly related to } P_C.$$

We also demonstrated that third order dispersion does not affect the critical power and that other nonlinear effects, such as self-steepening and intrapulse stimulated Raman scattering, can increase or decrease the critical power when combined with self-phase modulation. In addition, we have demonstrated that the critical power growth becomes smaller when the coupling constant is increased and the coupling coefficient dispersion is considered. Finally, we considered the case in which the temporal width T_0 is an independent variable and verified that P_C is crescent with T_0. As there is no analytical solution for the determination of the critical power when using ultrashort pulses, this result is useful to estimate it in applications such as logic gates and power bandwidth controllers, where the nonlinear effects are determinant to define the power-dependent switching. In addition, our results provide useful information for the construction of a more detailed model of the critical power in multi-core nonlinear coupler theory.

References

[1] T. A. Birks, P. J. Roberts, P. S. J. Russell, D. M. Atkin, and T. J. Shepherd, "Full 2-D photonic bandgaps in silica/air structures," *Electron. Lett.*, vol. 31, no. 22, pp. 1941–1943, Oct. 1995.

[2] J. Broeng, S. E. Barkou, A. Bjarklev, J. C. Knight, T. A. Birks, and P. S. J. Russell, "Highly increased photonic band gaps in silica/air structures," *Opt. Commun.*, vol. 156, nos. 4–6, pp. 240–244, 1998.

[3] P. Russell, "Photonic crystal fibers," *Science*, vol. 299, no. 5605, pp. 358–362, 2003.

[4] D. V. Skryabin, F. Luan, J. C. Knight, and P. S. J. Russell, "Soliton self-frequency shift cancellation in photonic crystal fibers," *Science*, vol. 301, no. 5640, pp. 1705–1708, 2003.

[5] J. Herrmann *et al.*, "Experimental evidence for supercontinuum generation by fission of higher-order solitons in photonic fibers," *Phys. Rev. Lett.*, vol. 88, no. 17, p. 173901, 2002.

[6] A. B. Aceves, M. Santagiustina, and C. De Angelis, "Analytical study of nonlinear-optical pulse dynamics in arrays of linearly coupled waveguides," *J. Opt. Soc. Amer. B, Opt. Phys.*, vol. 14, no. 7, pp. 1807–1815, 1997.

[7] M. Liu and K. S. Chiang, "Propagation of ultrashort pulses in a nonlinear two-core photonic crystal fiber," *Appl. Phys. B, Lasers Opt.*, vol. 98, no. 4, pp. 815–820, 2010. [Online]. Available: https://doi.org/10.1007/s00340-009-3870-8

[8] M. Liu and K. S. Chiang, "Nonlinear switching of ultrashort pulses in multicore fibers," *IEEE J. Quantum Electron.*, vol. 47, no. 12, pp. 1499–1505, Dec. 2011.

[9] T. Zhao, S. Lou, X. Wang, M. Zhou, and Z. Lian, "Ultrabroadband polarization splitter based on three-core photonic crystal fiber with a modulation core," *Appl. Opt.*, vol. 55, no. 23, pp. 6428–6434, 2016.

[10] W. Lu, S. Lou, and X. Wang, "Ultrabroadband polarization splitter based on a modified three-core photonic crystal fiber," *Appl. Opt.*, vol. 52, no. 35, pp. 8494–8500, 2013.

[11] G. Agrawal, *Nonlinear Fiber Optics*, 3rd ed. New York, NY, USA: Academic, 2001.

[12] P. V. Mamyshev and S. V. Chernikov, "Recent developments in the ultrashort pulse Raman effect in optical fibres," *Soviet Lightw. Commun.*, vol. 2, no. 2, pp. 97–111, 1992.

[13] R. H. Stolen and W. J. Tomlinson, "Effect of the Raman part of the nonlinear refractive index on propagation of ultrashort optical pulses in fibers," *J. Opt. Soc. Amer. B, Opt. Phys.*, vol. 9, no. 4, pp. 565–573, 1992.

[14] S. Trillo, S. Wabnitz, and G. I. Stegeman, "Nonlinear propagation and self-switching of ultrashort optical pulses in fiber nonlinear directional couplers: The normal dispersion regime," *IEEE J. Quantum Electron.*, vol. 25, no. 8, pp. 1907–1916, Aug. 1989.

[15] A. Araújo, A. Oliveira, F. Martins, A. Coelho, Jr., W. Fraga, and J. Nascimento, "Two all-optical logic gates in a single photonic interferometer," *Opt. Commun.*, vol. 355, pp. 485–491, Nov. 2015.

[16] A. Coelho, Jr., M. B. C. Costa, A. C. Ferreira, M. G. Da Silva, M. L. Lyra, and A. S. B. Sombra, "Realization of all-optical logic gates in a triangular triple-core photonic crystal fiber," *J. Lightw. Technol.*, vol. 31, no. 5, pp. 731–739, Mar. 1, 2013.

[17] M. B. C. Costa, A. M. Bastos, A. G. Coelho, Jr., C. Sobrinho, M. L. Lyra, and A. S. B. Sombra, "High contrast optical 'or' logic gates using a photonic crystal fiber modulated by PAM-ASK," *J. Opt. Commun.*, vol. 35, no. 2, pp. 85–94, 2014.

[18] P. Li, J. Zhao, and X. Zhang, "Nonlinear coupling in triangular triple-core photonic crystal fibers," *Opt. Exp.*, vol. 18, no. 26, p. 26828–26833, 2010.

[19] W. B. Fraga, J. W. M. Menezes, M. G. Da Silva, C. S. Sobrinho, and A. S. B. Sombra, "All optical logic gates based on an asymmetric nonlinear directional coupler," *Opt. Commun.*, vol. 262, no. 1, pp. 32–37, 2006.

[20] Q. Lai, M. Lanker, W. Hunziker, and H. Melchior, "Tunable wavelength-selection switch and multiplexer/demultiplexer based on asymmetric silica-on-silicon Mach–Zehnder interferometer," *Electron. Lett.*, vol. 34, no. 3, pp. 266–267, Feb. 1998.

[21] X. Sang, P. L. Chu, and C. Yu, "Applications of nonlinear effects in highly nonlinear photonic crystal fiber to optical communications," *Opt. Quantum Electron.*, vol. 37, no. 10, pp. 965–994, 2005.

[22] V. Finazzi, T. M. Monro, and D. J. Richardson, "Small-core silica holey fibers: Nonlinearity and confinement loss trade-offs," *J. Opt. Soc. Amer. B, Opt. Phys.*, vol. 20, no. 7, pp. 1427–1436, 2003.

[23] K. S. Chiang, "Coupled-mode equations for pulse switching in parallel waveguides," *IEEE J. Quantum Electron.*, vol. 33, no. 6, pp. 950–954, Jun. 1997.

[24] K. S. Chiang, "Propagation of short optical pulses in directional couplers with Kerr nonlinearity," *J. Opt. Soc. Amer. B, Opt. Phys.*, vol. 14, no. 6, pp. 1437–1443, 1997.

[25] K. S. Chiang, "Intermodal dispersion in two-core optical fibers," *Opt. Lett.*, vol. 20, no. 9, pp. 997–999, 1995.

[26] P. Shum, K. S. Chiang, and W. A. Gambling, "Switching dynamics of short optical pulses in a nonlinear directional coupler," *IEEE J. Quantum Electron.*, vol. 35, no. 1, pp. 79–83, Jan. 1999.

[27] P. M. Ramos and C. R. Paiva, "All-optical pulse switching in twin-core fiber couplers with intermodal dispersion," *IEEE J. Quantum Electron.*, vol. 35, no. 6, pp. 983–989, Jun. 1999.

[28] M. Liu, K. S. Chiang, and P. Shum, "Propagation of short pulses in an active nonlinear two-core optical fiber," *IEEE J. Quantum Electron.*, vol. 40, no. 11, pp. 1597–1602, Nov. 2004.
[29] K. Chiang *et al.*, "Experimental demonstration of intermodal dispersion in a two-core optical fibre," *Opt. Commun.*, vol. 143, nos. 4–6, pp. 189–192, 1997.
[30] P. Peterka, P. Honzatko, J. Kanka, V. Matejec, and I. Kasik, "Generation of high-repetition-rate pulse trains in a fiber laser through a twin-core fiber," *Proc. SPIE*, vol. 5036, pp. 376–382, Jul. 2003.

Alanio Ferreira de Lima was born in Iguatu, Brazil, in 1987. He received the B.Sc. degree in computer engineering from the Universidade Federal do Ceará–UFC–Campus Mucambinho, Sobral, Brazil, in 2016, where he is currently pursuing the M.Sc. degree in electrical and computer engineering with the Electrical and Computer Engineering Department.

Francisco Leonardo Bezerra Martins was born in Ipu, Brazil, in 1993. He received the B.Sc. degree in electrical engineering from the Universidade Federal do Ceará–UFC–Campus Mucambinho, Sobral, Brazil, in 2016, where he is currently pursuing the M.Sc. degree in electrical and computer engineering with the Electrical and Computer Engineering Department.

José Cláudio do Nascimento was born in Fortaleza, Brazil, in 1980. He received the B.Sc. degree in electrical engineering, the M.Sc. degree in teleinformatic engineering, and the Ph.D. degree in teleinformatic engineering from the Universidade Federal do Ceará–UFC, Brazil, in 2005, 2006, and 2009, respectively. He is currently a Professor of quantum information and optics communications with the Electric Engineering Department, Universidade Federal do Ceará–UFC–Campus Mucambinho, Sobral, Brazil.

Amarílio Gonçalves Coêlho, Jr. was born in Itapajé, Brazil, in 1981. He received the B.Sc. degree in physics from the Universidade Estadual Vale do Acaraú–UVA, Brazil, in 2006, and the M.Sc. degree in teleinformatic engineering and the Ph.D. degree in teleinformatic engineering from the Universidade Federal do Ceará–UFC, Brazil, in 2011 and 2016, respectively.